Nanoscale

Accepted Manuscript

This article can be cited before page numbers have been issued, to do this please use: J. S. Oh, J. Oh, D. SUNG and G. Yeom, *Nanoscale*, 2017, DOI: 10.1039/C7NR08078F.

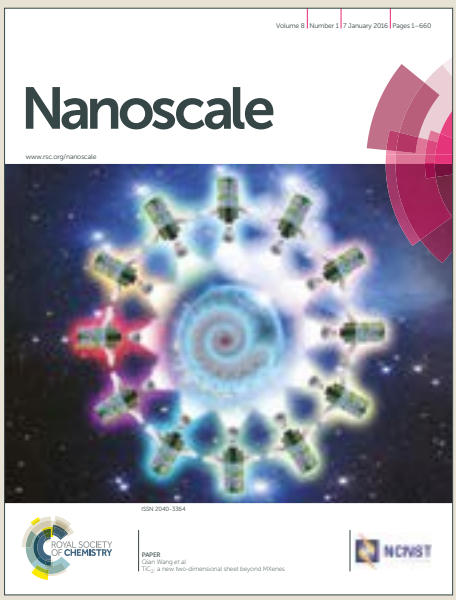

ROYAL SOCIETY OF CHEMISTRY

rsc.li/nanoscale

View Article Online
DOI: 10.1039/C7NR08078F

Nanoscale

ARTICLE

Fabrication of High-Performance Graphene Nanoplatelet-based Transparent Electrode via Self-Interlayer-Exfoliation Control

Received 00th January 20xx,
Accepted 00th January 20xx

DOI: 10.1039/x0xx00000x

www.rsc.org/

Jong Sik Oh[a], Ji Soo Oh[a], Da In Sung[a] and Geun Young Yeom*[a,b]

Graphene nanoplatelets (GNP) have attracted considerable attention due to their high yield and fabrication route that is scalable to enable graphene production. However, the absence of a means of fabricating a transparent and conductive GNP film has been the biggest obstacle to the replacement of pristine graphene. Here, we report on a novel means of fabricating uniform and thin GNP-based high-performance transparent electrodes for flexible and stretchable optoelectronic devices involving the use of an adhesive polymer layer (PMMA) as a GNP layer controller and by forming a hybrid GNP/AgNW electrode embedded on PET or PDMS. Relative to commercially available indium tin oxide (ITO) film on a PET substrate, a GNP-based electrode composed of hybrid GNP/AgNW on PET exhibits superb optical, physical, and electrical properties: a sheet resistance of 12 Ω/sq with 87.4 % transmittance, a variable work function from 4.16 to 5.26 eV, an ultra-smooth surface, a rate of resistance increase of only 4.0 % after 100,000 bending cycles, stretchability to 50 % of tensile strain, and robust stability against oxidation. Moreover, the GNP-based electrode composed of hybrid Cl-doped GNP/AgNW shows outstanding performance in actual organic light-emitting diodes (OLEDs) by exhibiting an increased current efficiency of 29.5 % and an increased luminous efficiency of 36.2 %, relative to the commercial ITO electrode on PET.

Introduction

Graphene has attracted considerable attention as a next-generation transparent electrode for flexible and stretchable optoelectronics as an alternative to indium tin oxide (ITO), due to features such as its superior intrinsic mobility, excellent Young's modulus, high thermal conductivity, and high optical transparency.[1-5] Therefore, many studies have set out to develop efficient and high-performance optoelectronic devices that use a graphene electrode fabricated using methods such as chemical vapor deposition (CVD).[6-11] However, despite the remarkable progress made in the past decade, this fabrication method inevitably incurs significant disadvantages, including high cost, long processing time, limited product size (micro-meter to centimeter range), unreliable transfer, and a high resultant sheet resistance (R_s).[12-15]

In order to fabricate high-quality transparent electrodes using CVD-grown graphene, it is essential to lower the R_s to the level of the ITO electrode. As a complementary approach, metallic nanowires or conductive polymers such as silver nanowires (AgNWs) or poly (3,4-ethylenedioxythiophene)-polystyrene sulfonate (PEDOT:PSS) has been used with CVD-grown graphene to lower the R_s.[16-18] However, these attempts focus solely on methods for lowering the R_s, and cannot address the fundamental manufacturing problems of CVD-grown graphene, including the physical and electrical properties that should be considered to manufacture transparent electrodes applicable to optoelectronics. Therefore, in order to use graphene as an industrially applicable transparent electrode, it is necessary to develop a new method that can overcome the limitations of the CVD graphene while maintaining excellent characteristics of graphene.

Recently, as alternatives to epitaxially grown and CVD-grown graphene, new graphene fabrication methods have been intensively investigated, not only to reduce cost and increase yield, but also to enable transfer-free and chemical functionalization using materials such as i) reduced graphene oxides (rGO) and ii) exfoliated graphene nanoplatelets (xGnP).[19-23] Due to the cohesive van der Waals (vdW) energy (5.9 kJ·mol^{-1}), which exists between the neighboring graphene sheets, graphite powder is more easily processed after forming an oxygen-containing functionality, known as 'graphene oxide (GO)', to form a single layer.[24] This functionalization process results in the hydrophilic affinity of GO and good dispersibility in many solvents.[25, 26] Thus, GO can be deposited on various substrates by using common methods such as drop-coating, spraying, and spin-casting, while a transparent electrode can be prepared by using a reduction process.[19, 27-32] However, the high operating temperatures and aggressive solvents used in the oxidation/reduction processes for the rGO attribute cause

[a] School of Advanced Materials Science and Engineering, Sungkyunkwan University, 2066 Seobu-ro, Jangan-gu, Suwon, Gyeonggi-do 16419, Republic of Korea. E-mail: ojs2k@skku.edu
[b] SKKU Advanced Institute of Nano Technology (SAINT), Sungkyunkwan University, 2066 Seobu-ro, Jangan-gu, Suwon, Gyeonggi-do 16419, Republic of Korea. E-mail: gyyeom@skku.edu

†Electronic Supplementary Information (ESI) available: See DOI: 10.1039/x0xx00000x

View Article Online
DOI: 10.1039/C7NR08078F

damage to rGO and produce relatively high values of R_s, ranging from 1 to 70 kΩ/sq with low light transparency (< 80 %) and, therefore, cannot be applied to an optoelectronic transparent electrode.[20, 33-37]

One other means of overcoming these problems associated with rGO is to use GNP, which is exfoliated from graphite to form graphene sheets with a thickness of a few layers. The GNP is a type of stacked 2-dimensional (2D) graphene sheet, having a plate size from the sub-nanometer to micro scale and a thickness from several to tens of nanometers.[38-41] To form GNP from graphite, appropriate acid or organic agents could be used as an intercalation material as these cause the exfoliation of GNP through the expansion of the graphite layers.[42-45] While the GNP is less susceptible to damage than rGO, the hydrophobicity of the GNP leads to agglomeration and dispersion problems which could significantly increase both the electrical resistivity and the surface roughness by forming ripples and wrinkles.[46] Therefore, it would not be possible to apply GNP electrodes to transparent conductive electrodes as a universal replacement for ITO, but they have been used to the applications such as Li-ion batteries,[47, 48] catalysts,[49] polymer composites,[50, 51] metal-matrix composites,[52] and electrical and thermal conductors.[53-55] However, the fabrication of transparent electrodes for flexible and stretchable optoelectronics with GNP will still be the most promising strategy and a significantly important challenge.

In the present study, we examined a new approach to the creation of a high-performance GNP-based transparent electrode for organic light emitting diodes (OLED). We focused on overcoming the problems associated with the fabrication of the GNP electrodes for use as transparent and flexible electrodes and found that uniform, thin, and layer-controlled GNP films are readily achievable by inserting an adhesive polymer, such as polymethyl methacrylate (PMMA), between the GNP and substrate. It is expected that, by using an adhesive PMMA layer on the substrate, pristine GNP, which is brush-coated directly onto the adhesive polymer, more easily adheres and produces a more uniform coating as a result of the enhanced adhesion force of the PMMA.

We also found that a hybrid electrode composed of GNP/embedded Ag nanowires (AgNW), fabricated as part of the present study, satisfies most of the essential requirements for the transparent electrodes used in practical optoelectronic applications. With the fabrication of a hybrid GNP/AgNW electrode, we obtained flexible and stretchable transparent electrodes that exhibit excellent physical and electrical properties that are even better than commercial ITO on PET types. Finally, we demonstrate that green flexible OLEDs fabricated with a hybrid GNP/AgNW electrode exhibit a luminance efficiency (LE) improvement of as much as 36.2 %, compared to flexible OLEDs fabricated with a commercial ITO electrode on PET. These results may give rise to entirely new ways of realizing flexible and stretchable optoelectronic devices for practical applications.

Experimental

Materials

AgNWs, measuring 25 ± 5 μm in length and 25 ± 5 nm in diameter, was purchased from NANOPYXIS, and diluted with 8–12 *ml* of isopropyl alcohol to 0.05 wt %. The GNP powder was purchased from Angstron Materials, N002-PDR (average *x-y* dimensions ≤ 10 μm, average number of layers of graphene ≤ 3; exfoliated, carbon content ≥ 95 %, oxygen content ≤ 2.5 %, hydrogen content ≤ 2.5 %, nitrogen content ≤ 0.5 %).

GNP coating methods

Schematic illustrations of each GNP coating method (spray coating, bar spreading, brush coating onto bare glass, and brush coating onto adhesive polymer) are shown in Fig. S1. Fig. S1a shows GNP spray coating using an air brush. A GNP dispersed solution (Angstron Materials, N002-PDR, 4 mg GNP in 50 *ml* isopropanol) was prepared using a sonication process for 1 h. The size of the moving X–Y stage was 15 cm × 15 cm, and the stage temperature was maintained at 65 °C while spraying GNP to remove the isopropanol. Fig. S1b shows the spin coating process where GNP dispersed in the isopropanol can be spread into a flat film. Figure S1c, d shows the dry brush coating process onto bare glass and onto polymethyl methacrylate (PMMA; 950 PMMA C4 resist, Microchem) coated glass, respectively. A 30 mm × 30 mm soda lime glass was used as the substrate for the coating of GNP and PMMA. PMMA was used as the adhesive and detachable base layer for the deposition of the flexible and stretchable electrode on the glass substrate. The PMMA was spin-coated onto the glass at 4000 rpm for 40 s, and subsequently baked on a hotplate at 140 °C for 2 min to remove the solvent. The thickness of deposited PMMA was ~ 130 nm. The GNPs were brush-coated onto the PMMA surface ten times to produce a coating that was a few layers thick.

Fabrication of GNP/AgNW electrode

Fig. S2 shows the fabrication process of the GNP/AgNW electrode in detail. A solution of AgNW was spin-spray-coated onto the GNP using a spray gun (SPARMAX GP-35), while the glass substrate was spun at 4000 rpm to achieve a more uniform AgNW coating. The fabricated electrode was patterned using a stainless shadow mask similar to the patterned metal mask employed in the fabrication of an OLED device. The patterning was done during the brush coating of the GNP and spin-spray-coating of the AgNW. For the commercial flexible ITO electrode, a PET substrate deposited with a 300-nm thick ITO film (Fine Chemical Industry) was used.

To embed the AgNW and GNP/AgNW electrodes in the flexible polymer substrate, an UV-curable resin (NIP-K28, ChemOptics), which is a colorless clear liquid with an UV exposure tolerance of > 1400 mJ/cm^2 and a viscosity of 11 CPS, was drop-coated onto the AgNW/GNP/PMMA/glass substrate composite. A metal-halide UV lamp rated at 80 W/cm^2, 8 A with a peak intensity wavelength of 260 nm was then used to cure the UV resin for 2 min. The thickness of the flexible substrate, including the GNP/AgNW and UV resin, was about 25 μm. To increase the thickness of the flexible substrate in some

View Article Online
DOI: 10.1039/C7NR08078F

samples, a 200-μm PET film was attached to the UV resin before curing and the two materials were cured together to form a flexible electrode on PET. To embed the hybrid electrode in the stretchable substrate, instead of the UV resin, we prepared a polydimethylsiloxane (PDMS) (Sylgard 184, Dow Corning) by mixing the base and curing agent at a ratio of 10:1. After all the air bubbles in the liquid PDMS were cleared, we spin-coated the liquid PDMS onto the AgNW/GNP/PMMA substrate for 30 s at 500 rpm and then cured it at 60 ℃ for 4 h to form cross-linked solid PDMS.

To detach the flexible electrode from the glass substrate, the entire system was dipped into deionized (DI) water at 90 °C. The permeation of the DI water into the interface between the PMMA layer and the glass substrate led to the instant separation of the flexible electrode from the glass substrate. Any PMMA that remained on the detached flexible substrate was easily removed by dipping the substrate into acetone for a few minutes. This exposed the GNP surface of the flexible transparent electrode.

Doping process

The GNP surface of the hybrid GNP/AgNW electrode was doped by spin-coating with an $AuCl_3$ solution or by exposure to Cl_2 plasma using a plasma processing system. In the former case, a 10-mM $AuCl_3$ solution was prepared using nitromethane (CH_3NO_2, ≥ 95 %), and the solution was deposited on the electrode by spin coating for 30 s at 2000 rpm. In the latter case, an inductively coupled plasma (ICP) system operating at 13.56 MHz was employed. To avoid damage to the surface of the hybrid electrode during the doping, two grounded mesh grids were installed between the ICP source and the substrate. The electrode was doped with the Cl_2 plasma for 10 s at 10 mTorr, 60 sccm, and a radio frequency (RF) power of 20 W. The ICP system and the possible Cl_2 plasma doping mechanism of the GNP/AgNW are shown in Fig. S3.

OLED fabrication

The OLED devices were fabricated using five different types of patterned anodes, namely, ITO on PET, embedded AgNW on PET, undoped GNP/AgNW on PET, $AgCl_3$-doped GNP/AgNW on PET, and Cl_2-doped GNP/AgNW on PET. The R_s values of all the electrodes were maintained at ~ 12 Ω/sq.

The following layers were sequentially deposited on the anode of each OLED device by using a thermal evaporator (JBS International Co., Ltd.) after masking with a stainless-steel shadow mask: (1) a hole transport layer (40-nm): N,N′,-bis-(1-naphthyl)-N,N′-diphenyl1–1′-biphenyl-4,4′-diamine; (2) an exciton blocking layer (10-nm): tris(4-carbazoyl-9-ylphenyl) amine (TCTA); (3) an emitting layer (30-nm): tris(phenylpyridine) iridium (Ir(ppy)3)-doped N4,4′-bis(-carbazolyl)-1,1′-biphenyl (CBP); and (4) an electron transport layer (20-nm): 4-7-diphenyl-1,10-phenanlhroline (BPhen). The evaporation rate was around 1–2 Å/s. The cathode layer was a 100-nm Al layer deposited by thermal evaporation using a separate shadow mask and an evaporation rate of 2 Å/s.

Measurements

The textures and morphologies of the electrodes were observed by a field emission scanning electron microscope (FE-SEM) (Hitachi S-4700), while an ultraviolet visible (UV-Vis) spectroscope (UV-3600, Shimadzu) was used to compare the optical transmittances of the different electrodes. The sheet resistance R_s was measured using the four-point method (Keithley 2000, Keithley). An atomic force microscope (AFM) (XE-100, PSIA Co.) and a 3-dimensional (3D) profiler (Bruker DXT-A, Bruker Co.) were used to measure the surface roughness of the GNP-coated surface and embedded hybrid GNP/AgNW electrode. The work functions of the electrodes were measured using an ultraviolet photoelectron spectroscope (UPS) (PHI 5000 VERSAPROBE, ULVACPHI). The current density-voltage (J-V) and luminance-voltage (L-V) characteristics were measured using a programmable electrometer with a built-in current-voltage measurement unit (M6100, McScience) and a spectro-radiometer (CS-1000, Minolta).

Results and Discussion

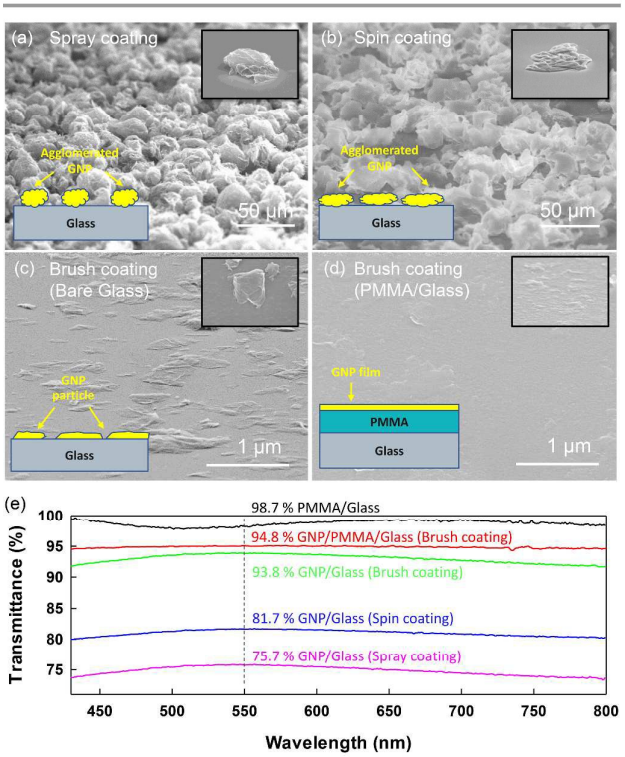

Fig. 1 SEM images (tilt angle: 45 °) and optical transmittances for different GNP coating methods. The coating was repeatedly processed for 6 times. a) GNP spray-coated onto bare glass surface. b) GNP spin-coated onto bare glass surface. c) GNP brush-coated onto bare glass surface. d) GNP brush-coated onto PMMA coated glass surface. e) Optical transmittance and sheet resistance of GNP films coated on different substrate conditions. (Bare glass transmittance was set to the base-line)

View Article Online
DOI: 10.1039/C7NR08078F

Scanning electron microscopy (SEM) revealed different surface morphologies of the GNP-coated surfaces produced by spray coating, spin coating, and brush coating on glass susbtrates, and brush coating on adhesive polymer (PMMA) coated glass susbstrate, as shown in Fig. 1a–d. The spray-coated GNP (Fig. 1a) has an irregular arrangement, and each agglomeration of nanoplatelets exhibits a shape like a heavily crumpled piece of tissue. The appearance of a spray-coated single GNP particle can be seen in detail in the right-hand inset of Fig. 1a. The GNP which is neither transformed into graphene oxide (GO) or dispersed by the solvent, as shown in Fig. 1a, easily agglomerates under the influence of the van der Waals (vdW) force. Therefore, GNP was coated using a spin coater to increase horizontal force towards surface direction and to deform GNP into a flat film, as shown in Fig. 1b. In Fig. 1b, it can be seen that each GNP particle was more extruded in the horizontal direction but the GNP coated surface was still very rough. Also, for spray coating and spin coating, the thickness of the GNP film could not be controlled, and the GNP coverage uniformity was still poor because the horizontal force to separate the GNP layers is insufficient and the adhesive force between the GNP and the glass is very low. For uniform GNP coating onto a substrate while keeping the coating thickness thin, we adopted the brush-coating method. To avoid the agglomeration effect and to better control the GNP layer thickness, we brush-coated the GNP on the glass substrates without using any dispersive solvents or liquids. The results of the dry-brush coating process are shown in Fig. 1c and Fig. 1d. In the case of brush coating the GNP onto a bare glass surface, as shown in Fig. 1c, because of the weak vdW force between the GNP and silicon dioxide, the nanoplatelet itself did not easily stick to the substrate and the GNP was partially agglomerated in some areas even though the multiple GNP layers were split into a few thin layers. Therefore, the GNP failed to uniformly cover the glass surface when the brush-coating method was applied. Fig. 1d shows the surface morphology of brush-coated GNP on PMMA-coated bare glass. Unlike the case of forming a GNP film on a bare glass surface, due to the higher binding energy between the GNP and PMMA, the horizontal movement of the brush induces self-exfoliation of interlayer structures of GNP particles except for the surface bonded with PMMA (self-interlayer-exfoliation). Thus, a fully covered and finely layer-controlled coating was obtained.

When the optical transmittance was measured as a function of wavelength under various coating conditions, as shown in Fig. 1e, the GNP coating on the PMMA exhibited the highest transparency (94.8 % at 550 nm) of all the coatings produced using the different processes, and the entire surface is fully covered with GNP. The higher optical transmittance of the GNP coating on PMMA, relative to the coatings produced using other methods, appears to be related to the more uniform and thinner GNP coating on the PMMA surface. Therefore, it is found that uniformly coated, thin GNP films (with an average of two monolayers) can be fabricated when the GNP is brush-coated onto a substrate coated with adhesive polymer.

To compare the surface roughness of GNP-coated surface for different coating methods and substrate conditions, we measured the root mean square (RMS) roughness of each GNP-coated surface by using a 3D profiler and AFM. The results are shown in Fig. 2. Fig. 2a-c show the 3D profiler images of the GNP-cated surface by using spray coating, spin coating, and brush coating methods, respectively. The RMS roughness values of the GNP coated with the spary coating method and the spin coating method were 4.5 and 3.8 µm, respectively, therefore, the RMS roughness of the spin-coated GNP was measured to be slightly lower. It is assumed that the horizontal directional force due to the centrifugal force generated by the spray coating method decreased the RMS roughness compared to spray coating method and, as can be observed in Fig. 1e, the spin-coated GNP film has higher light transmittance than the spray-cated GNP film. However, as shown in Fig. 2c, brush-coated GNP film on PMMA/glass had a very smooth surface, so that it is difficult to obain an accurate roughness value with the 3D profiler. Therefore, the roughness of the brush-coated GNP was also analyzed with AFM and the result is shown in Fig. 2d. As shown in Fig. 2d, the R_q of brush-coated GNP film was about 2.5 nm, which is ~ 0.056 % and 0.066 % compared to spray-coated GNP and spin-coated GNP, respectively.

Fig. 3a shows the manufacturing process of hybrid GNP/AgNW-based flexible/strechable transparent electrodes. In the case of the GNP dry brush-coating only, a thin and uniform GNP film could be prepared on PMMA coated glass substrates. However, due to the many physical defects present in GNP and the high contact resistance, it is inappropriate to use alone as a transparent electrode, because of its extremely high sheet resistance. Therefore, we developed a method of fabricating a GNP/AgNW hybrid transparent electrode with an embedded structure to reduce the R_s of GNP to the ITO level

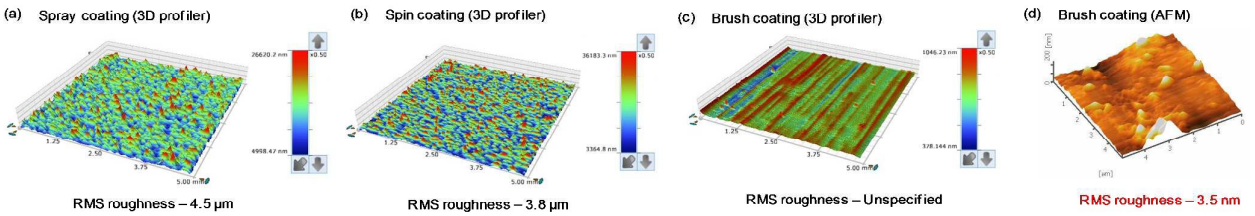

Fig. 2 3D profiler and AFM images for different GNP coating methods. Each coating was processed on PMMA coated glass. a) 3D profiler image of GNP surface coated with spray coating method. b) 3D profiler image of GNP surface coated with spin coating method. c) 3D profiler image of GNP surface coated with brush coating method. d) 3D AFM image of GNP surface coated with brush coating method. Due to high surface roughness for spray coating and spin coating, 3-D profiler was used to measure the surface roughness.

View Article Online
DOI: 10.1039/C7NR08078F

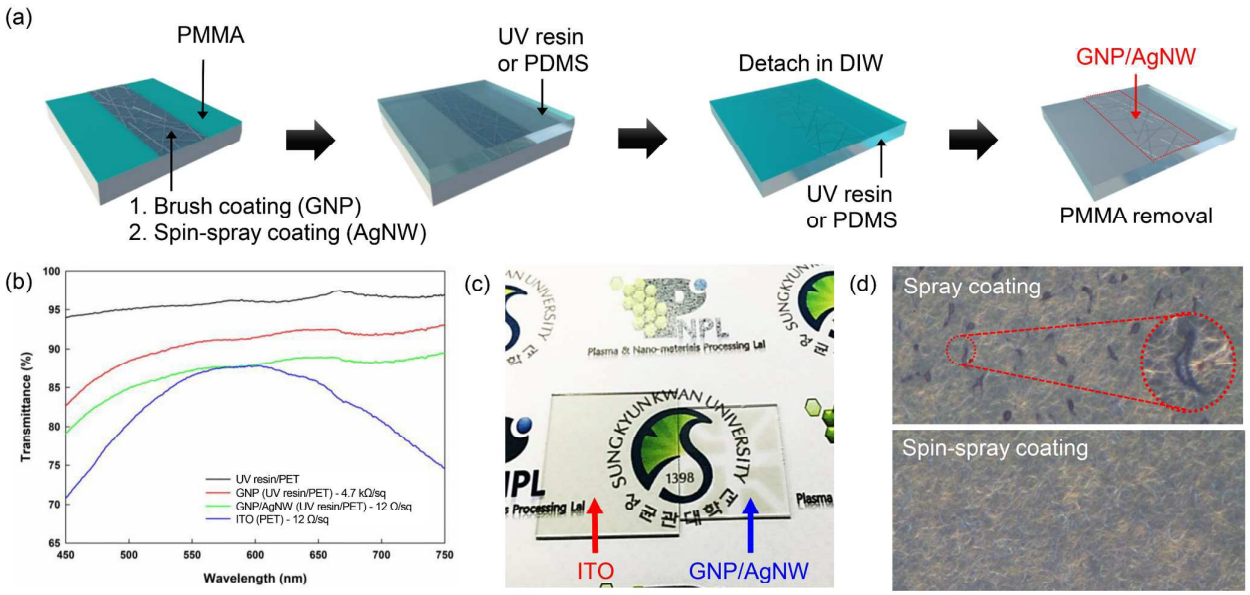

Fig. 3 a) Schematic diagram of a GNP/AgNW hybrid electrode embedded in a flexible and stretchable substrate. b) Optical transmittances of various electrodes in the visible wavelength region. c) Optical images of the ITO on PET and the patterned GNP/AgNW-embedded transparent flexible electrode on PET with the similar resistivity of 12 Ω/sq. d) Optical microscopic images (20 times of coating) of a conventional spray coating process and a spin-spray coating process of AgNW used in this study.

and to simultaneously make the surface ultra-smooth. After GNP dry brush coating on PMMA coated glass substrate, a solution of AgNW was subsequently spin-sprayed uniformly onto the GNP layer to form a GNP/AgNW hybrid electrode. Next, the GNP/AgNW hybrid electrode was drop-coated with a UV-curable resin or PDMS. This was done to embed the GNP/AgNW hybrid electrode in a transparent flexible or stretchable substrate. To separate the GNP/AgNW electrode embedded in the UV resin or PDMS, the sample was dipped into heated DI water. Given the hydrophilicity of the glass surface and the hydrophobicity of the PMMA surface, the two materials spontaneously separated at their interface. The PMMA that remained on the GNP/AgNW electrode surface was subsequently removed by acetone cleaning. Since the GNP/AgNW electrode is fabricated on the PMMA layer, the surface roughness of the GNP/AgNW electrode is determined by that of the PMMA layer. Therefore, in this process, the PMMA layer enables (1) the separation of the electrode from the substrate, and leads to (2) the ultra-smoothness of the surface. Fig. 3b shows the optical transmittances of the GNP/AgNW hybrid electrode and ITO film on PET substrates in the visible wavelength region for the sheet resistances of 12 Ω/sq. The optical transmittances of UV resin/PET substrate and dry-brush-coated GNP were also measured and are shown for comparison. The sheet resistance of a common OLED anode is generally no more than 20 Ω/sq. Therefore, the optical transmittances of the AgNW and GNP/AgNW hybrid electrodes with sheet resistances of ≤ 20 Ω/sq were used for OLED device fabrication. The sheet resistance of the commercial ITO on a PET substrate was around 12 Ω/sq. In the case of the GNP/UV resin/PET electrode and spin-spray coated AgNW/GNP/UV resin/PET electrode, sheet resistance of 4.7 kΩ/sq and 12 Ω/sq were achieved, with corresponding transmittances of 91.6 % and 87.4 % at a wavelength of 550 nm, respectively. The differences between the transmittances of the hybrid electrodes and those of the GNP without AgNW correspond to the optical transmittance of the AgNW, indicating that the sheet resistance of the hybrid electrodes is mostly produced by the AgNW. The optical transmittance of the ITO on PET at a wavelength of 550 nm was 86.5 %, which is similar to that of the investigated GNP/AgNW, although it was generally comparatively lower at other wavelengths. Fig. 3c shows optical microscope images of the ITO on PET and the patterned GNP/AgNW electrode embedded in UV resin. Fig. 3c confirms the similar optical transmittance characteristics of the two electrodes in addition to the same resistivity of 12 Ω/sq. Fig. 3d shows the uniformity of the spin-spray-coating process used during AgNW coating. The AgNW produced by a conventional spray coating method exhibited dark spots which are related to the irregular coating (agglomerated during the evaporation of AgNW-dispersed solution) in addition to the variation in the optical transmittance for a similar sheet resistance. However, when the AgNW was applied by the spin-spray coating, in which AgNWs are sprayed while spinning the substrate, a very uniform coating without dark spots and a consistent optical transmittance was obtained.

The transparency, sheet resistance, and surface roughness of GNP-based transparent electrodes reported in the literature are summarized in Table 1.[20, 56-62] Our results shows the lowest R_s and R_q values at the similar transparency (550 nm), indicating that brush-coated GNP with AgNW embedded in the substrate is the most promising electrode structure with excellent properties for optoelectronic devices.

View Article Online
DOI: 10.1039/C7NR08078F

Table 1 - Transparency, sheet resistance and surface roughness of GNP-based transparent electrodes obtained by other research groups

Author	Transparency at 550 nm (%)	Sheet resistance (Ω/sq)	Surface roughness (nm, R_a or R_q)
J. S. Park *et al.*, *ACS Appl. Mater. Interfaces*[56]	80	1,400	Unspecified
Q. Zheng *et al.*, *ACS nano*[57]	90	459	Unspecified
V. H. Phan *et al.*, *Carbon*[58]	84	2,200	Unspecified
S. J. Wang *et al.*, *Carbon*[59]	80	1,000-2,000	Unspecified
D. W. Lee *et al.*, *J. Mater. Chem.*[60]	86	8,600	Unspecified
Q. B. Zheng *et al.*, *Carbon*[61]	81.7	1,598	3.08 (R_q)
H. A. Becerril *et al.*, *ACS nano*[20]	80	100-1,000	5.3 (R_a)
J. Wang *et al.*, *Adv. Mater.*[62]	78	840	1.3 – 4 (R_q)
Our results	87.4	12	0.64 (R_q)

Fig. 4a shows the work functions of different relevant materials, namely, ITO, AgNW, GNP/AgNW, $AuCl_3$-doped GNP/AgNW ($AuCl_3$/GNP/AgNW), and Cl_2 plasma-doped GNP/AgNW (Cl_2/GNP/AgNW), as measured by UPS. The OLED devices tend to have a very high occupied molecular orbital (HOMO) energy (> 5.0 eV) on the anode side; therefore, to achieve the lowest possible energy barrier between the anode and the OLED material, it is necessary to use a material with a higher work function as the anode. As shown in Fig. 4a, ITO, which is generally used for the anodes of OLED devices, has a higher work function of 4.6 eV, compared to the 4.16 eV of AgNW. Therefore, the use of AgNW instead of ITO as the OLED anode can increase the contact resistance and thus can degrade the device characteristics. The GNP/AgNW electrode used in the study has the work function of 4.5 eV related to the work function of graphene itself, and which is comparable to that of ITO. The GNP/AgNW electrode has 4.5 eV becasuse the outside of the electrode facing the OLED is the graphene. However, when the surface of GNP is doped with p-type dopants using $AuCl_3$ and Cl_2 plasma, the work function is

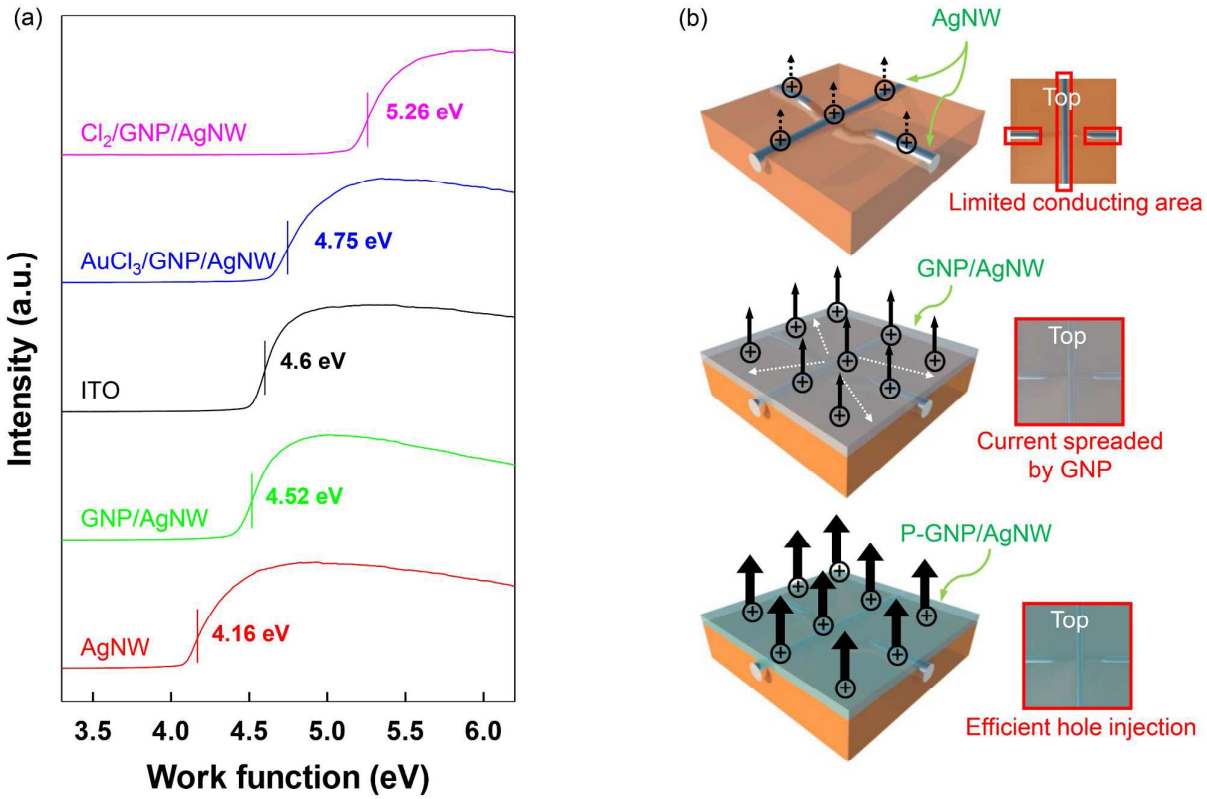

Fig. 4 a) Work functions and the graphical drawings of various transparent electrodes fabricated for OLED devices. a) Work functions of various materials such as ITO, AgNW, GNP/AgNW, $AuCl_3$ doped GNP/AgNW ($AuCl_3$/GNP/AgNW), and Cl_2 plasma doped GNP/AgNW (Cl_2/GNP/AgNW) measured using UPS. b) Graphical drawings of hole injection from AgNW, GNP/AgNW, and doped-GNP/AgNW. The density of (+) symbol and the thickness arrow indicate the exposed electrode area and hole injection efficiency, respectively.

View Article Online
DOI: 10.1039/C7NR08078F

increased to 4.75 eV for $AuCl_3$ and to 5.26 eV for Cl_2 plasma. The chlorine gas plasma thus increases the work function by as much as 0.74 eV.

Fig. 4b is a graphical illustration showing the conducting area and hole injection efficiency of AgNW, GNP/AgNW, and doped-GNP/AgNW electrodes. In the AgNW electrode, even if it has the same R_s, there are many non-conducting regions with no current flow between the wires. Since the GNP is composed of graphene which has excellent mobility, the GNP layer used with the AgNW electrode can remove the non-conducting regions and induce current flow over the entire substrate. Moreover, by applying the doping process to the GNP layer, it is possible to increase the work function and increase the hole injection efficiency.

The surface images and roughnesses of the GNP and AgNW after the sequential coating to a PMMA-coated glass substrate were measured by SEM and AFM. Fig. 5 shows the results after dry brush coating of the GNP on the PMMA (a, d), after the spin-spray coating of the AgNW on the GNP-coated PMMA (b, e), and of the final embedded GNP/AgNW electrode (c, f). As shown in Fig. 5a, the GNP coating on the PMMA surface appears smooth because of the use of the dry brush coating. The AFM result shown in Fig. 5d indicates an RMS surface roughness of ~ 3.51 nm, which is possibly due to the superimposition of the edges of the GNP during the coating. The peak-to-valley roughness (R_{P-V}), however, was as high as 53.0 nm. When the AgNW was directly spin-spray-coated onto the GNP/PMMA, the surface roughness was further increased by the diameter of the AgNW and the crossover, as shown in Fig. 5b. The RMS surface roughness and R_{P-V} were 15.4 and 214.4 nm, respectively, as shown in Fig. 5e. However, in the case of the embedded GNP/AgNW hybrid electrode, formed by detaching the flexible substrate from the glass substrate as shown in Fig. 5c, and e, the surface of the electrode was extremely smooth, having an RMS roughness and R_{P-V} of 0.64 and 8.47 nm, respectively. Therefore, relative to the GNP and AgNW coatings on a substrate, the embedded hybrid electrode exhibited excellent surface smoothness, which is required for the fabrication of stable OLED devices. Given that the ultimate goal is the application to flexible and stretchable displays, the flexibility and stretchability of the hybrid GNP/AgNW electrodes formed on PET and PDMS were compared with that of an ITO electrode on PET. The variations in the resistances of these electrodes were examined as the electrodes were bent to a radius r of 5 mm and released back to 27 mm, to investigate the restorability of the resistance. Fig. 6a, b shows the variation in the resistances of the two electrodes, hybrid GNP/AgNW electrode on PET and an ITO electrode on PET, during tensile and compressive bending, respectively. The two electrodes had the same sheet resistance of 12 Ω/sq and similar optical transmittances at 550 nm, as shown in Fig. 3b. In Fig. 6a, b, we can see that the resistance of the ITO on PET electrode did not significantly change as a result of the initial tensile and compressive bending to a radius of 7 mm. However, when the bending radius was decreased to 5 mm, the resistance was rapidly increased by about 29.8 % and 82.5

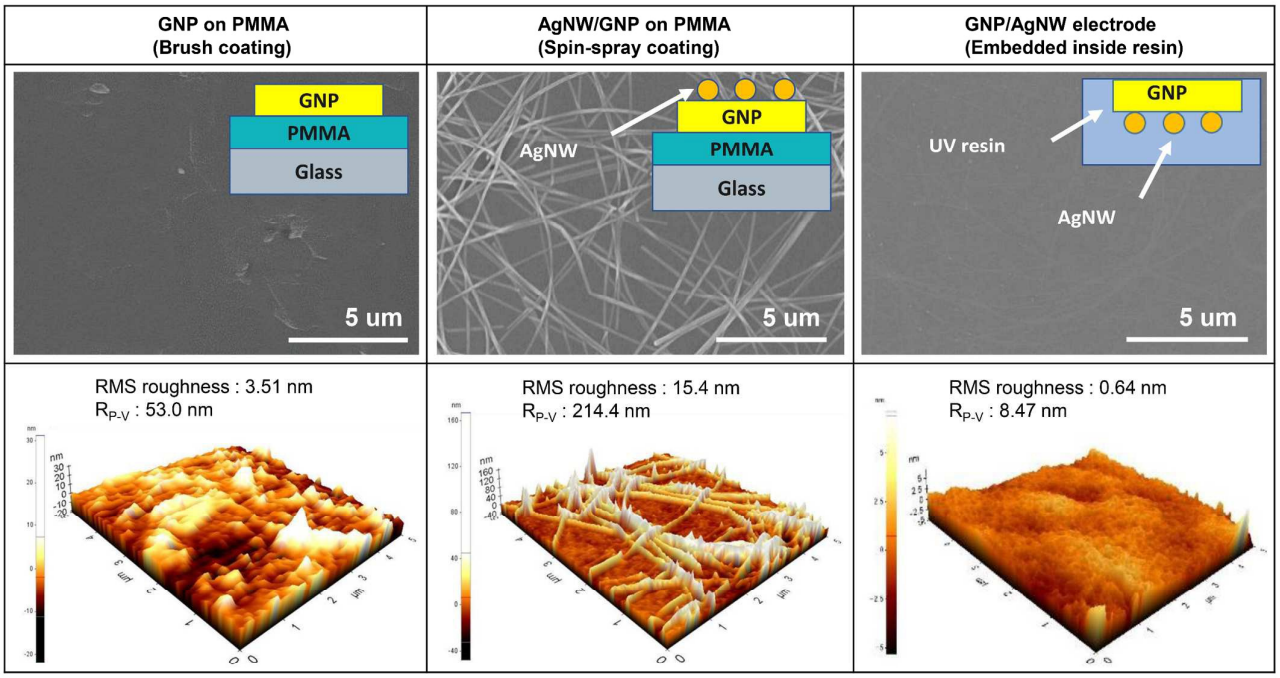

Fig. 5 SEM and AFM surface roughness after GNP brush-coating on PET (a and d), after AgNW spray-coating on GNP coated PET (b and e), and for the final GNP/AgNW-embedded electrode (c and f). Compared to the GNP and AgNW coated on the substrate, the embedded GNP/AgNW hybrid electrode exhibited excellent surface smoothness not only for RMS roughness but also for peak-to-peak roughness (R_{P-V}).

View Article Online
DOI: 10.1039/C7NR08078F

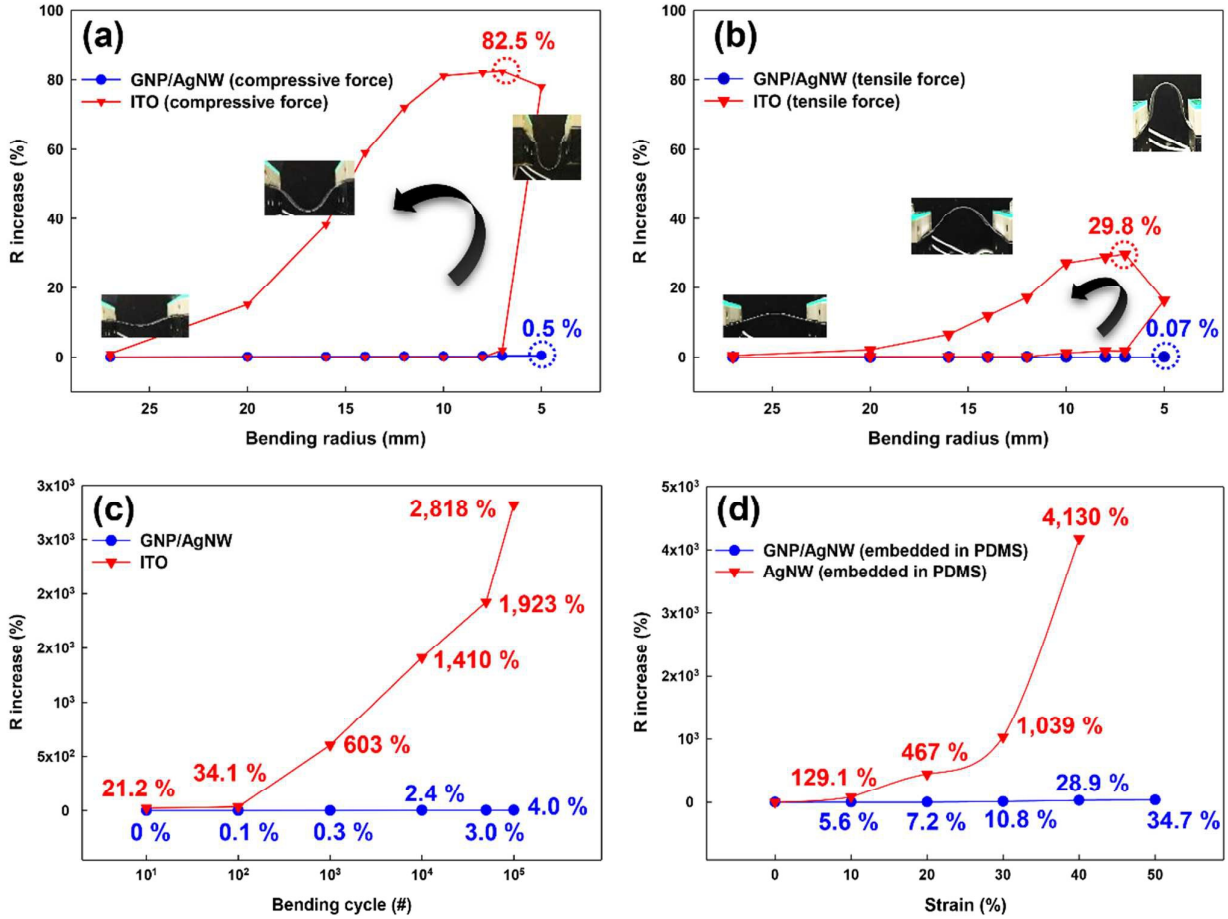

Fig. 6 Flexibility and stretchability of the GNP/AgNW-embedded electrode. Changes of electrical resistance during a) compressive and b) tensile bending, respectively, from 27 mm to 5 mm and back to 27 mm of bending radius. c) Changes of resistance during the cyclic bending for GNP/AgNW hybrid electrode on PET and ITO on PET. d) Changes of resistance during the longitudinal strain force applied to GNP/AgNW hybrid electrode on PDMS and AgNW on PDMS. Both GNP/AgNW hybrid electrode and the ITO electrode which have the similar sheet resistance of 12 Ω/sq and similar optical transmittance at 550 nm as shown in Fig. 2b were tested.

% during the tensile and compressive bending, respectively, possibly due to the cracking of the ITO on the bent PET surface. When the bending force was released, the resistance was mostly restored to the initial value, possibly by the reconnection of the cracked ITO during the shrinkage of the PET substrate. On the other hand, in the case of the GNP/AgNW hybrid electrode on PET, the resistance was changed by no more than 0.07 % and 0.5 % under tensile bending and compressive bending, respectively, even when the bending radius was decreased to 5 mm. This indicated practically no change in the sheet resistance, which is attributable to the high flexibility of the GNP and AgNW embedded in the polymer. Fig. 6c shows the variation in the resistances of the hybrid GNP/AgNW and ITO electrodes on PET during cyclic bending, performed to evaluate the reliability of the restorative capabilities of the two electrode types. Each electrode type was subjected to 100,000 bending cycles; each consisting of bending from a radius of 27 mm to one of 5 mm, and then back to 27 mm. The ITO electrode exhibited a resistance increase of about 21.2 % after the 10th bending cycle, and a rapid increase after hundreds of cycles. After 100,000 cycles, the resistance had increased by 2,818 %. This was attributed to the brittleness of the electrode, which is a serious source of unreliability. However, the GNP/AgNW hybrid electrode exhibited a resistance increase of only around 4 % after 100,000 cycles, indicating outstanding flexibility. In addition, for stretchable optoelectronic applications, we measured the stretchability of the GNP/AgNW electrode. Fig. 6d shows the change in R_s measured while tensile strain was applied to the AgNW and GNP/AgNW electrodes embedded in PDMS. In addition to the electrical advantages described in Fig. 4, above, the advantage of physical stretchability was found through the observation of the R_s change which varies with the longitudinal stretching strain for the AgNW and the GNP/AgNW electrodes embedded in PDMS. As shown in Fig. 6d, the R_s of the AgNW embedded in PDMS was rapidly increased with the tensile strain, exhibiting an increase of about 4,130 % at 40 % strain. When the strain was increased to 50 %, we assumed that the contacts between the AgNWs had broken because the R_s could not be measured. However,

View Article Online
DOI: 10.1039/C7NR08078F

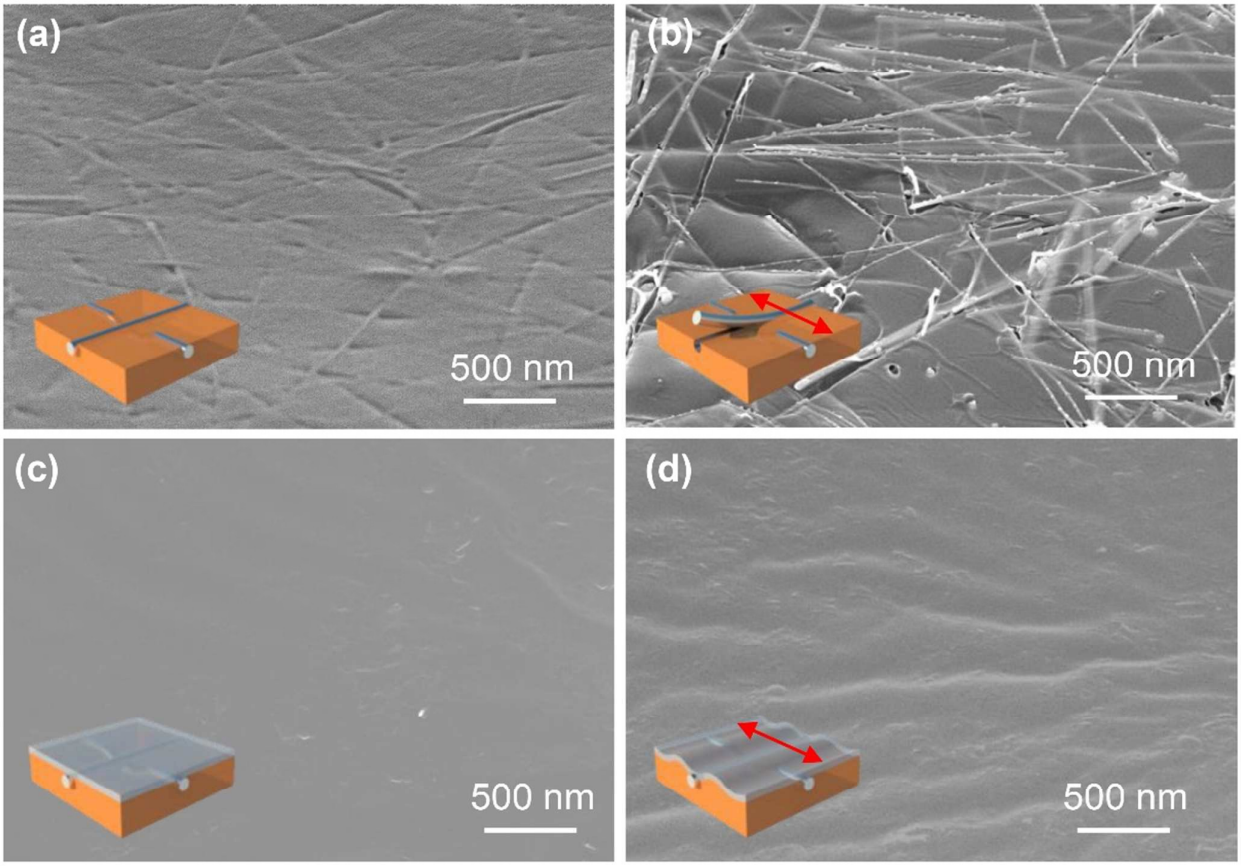

Fig. 7 Effect of GNP to AgNW embedded in PDMS on stretchability: schematic and SEM images of a) un-stretched AgNW electrode embedded in PDMS; b) recovered AgNW electrode embedded in PDMS after 40 % strain to the longitudinal direction; c) un-stretched GNP/AgNW electrode embedded in PDMS; d) recovered GNP/AgNW electrode embedded in PDMS after 40 % strain to the longitudinal direction.

unlike the AgNW embedded PDMS, the R_s of the GNP/AgNW embedded in PDMS was increased by only 34.7% even if the strain increased to 50 %.

To analyze the superior stretchability of the GNP/AgNW hybrid electrode, relative to a AgNW electrode, we observed the surface morphology of the 40 %-stretched AgNW electrode and GNP/AgNW electrode by using SEM. The results are shown in Fig. 7. The surface morphologies observed before stretching the AgNW and GNP/AgNW electrodes embedded in PDMS substrate are shown in Fig. 7a and c, respectively. In the AgNW electrode embedded in PDMS, since there is no flat layered structure like GNP, the AgNWs were exposed on the surface. Fig. 7b, d show the results of the recovered surface morphologies after applying a 40 % longitudinal stretching strain to the AgNW and GNP/AgNW electrodes embedded in PDMS, respectively. In the AgNW electrode embedded in PDMS, many AgNWs were found to be protruding from the substrate after the stretching strain was applied to the substrate. On the other hand, for the GNP/AgNW hybrid electrode embedded in PDMS, no AgNWs were found to protrude from the substrate. Rather, only wrinkles appeared on the surface, as a result of the difference in the expansion coefficients of the GNP and the PDMS. Since the connection of the AgNWs is an important factor determining the resistance of an electrode, it is thought that the GNP layer plays a major role in preventing the detachment of the AgNWs from the substrate and enhancing the physical stability when stretch strain is applied.

Finally, to demonstrate the optoelectrical performance of the GNP/AgNW electrodes, flexible green OLED devices were fabricated and analyzed using a range of transparent electrodes. The right-hand inset of Fig. 8a shows the structure of the fabricated OLED device. In addition, to accurately analyze the advantages of the GNP/AgNW hybrid electrode relative to a conventional AgNW electrode, undoped and doped GNP/AgNW hybrid electrodes were used. Furthermore, to determine the applicability of the GNP/AgNW hybrid electrodes to next-generation flexible electrodes, the results were compared with OLED devices fabricated with a conventional ITO electrode on PET. The sheet resistance of all the investigated electrodes was maintained at 12 Ω/sq.

Fig. 8a shows the current densities of the OLEDs as a function of the voltage. Due to the increase in the work function of the GNP/AgNW hybrid electrode by doping with $AuCl_3$ and Cl_2 plasma from 4.5 eV to 4.75 eV and 5.26 eV, respectively, the corresponding OLED devices fabricated with GNP/AgNW

View Article Online
DOI: 10.1039/C7NR08078F

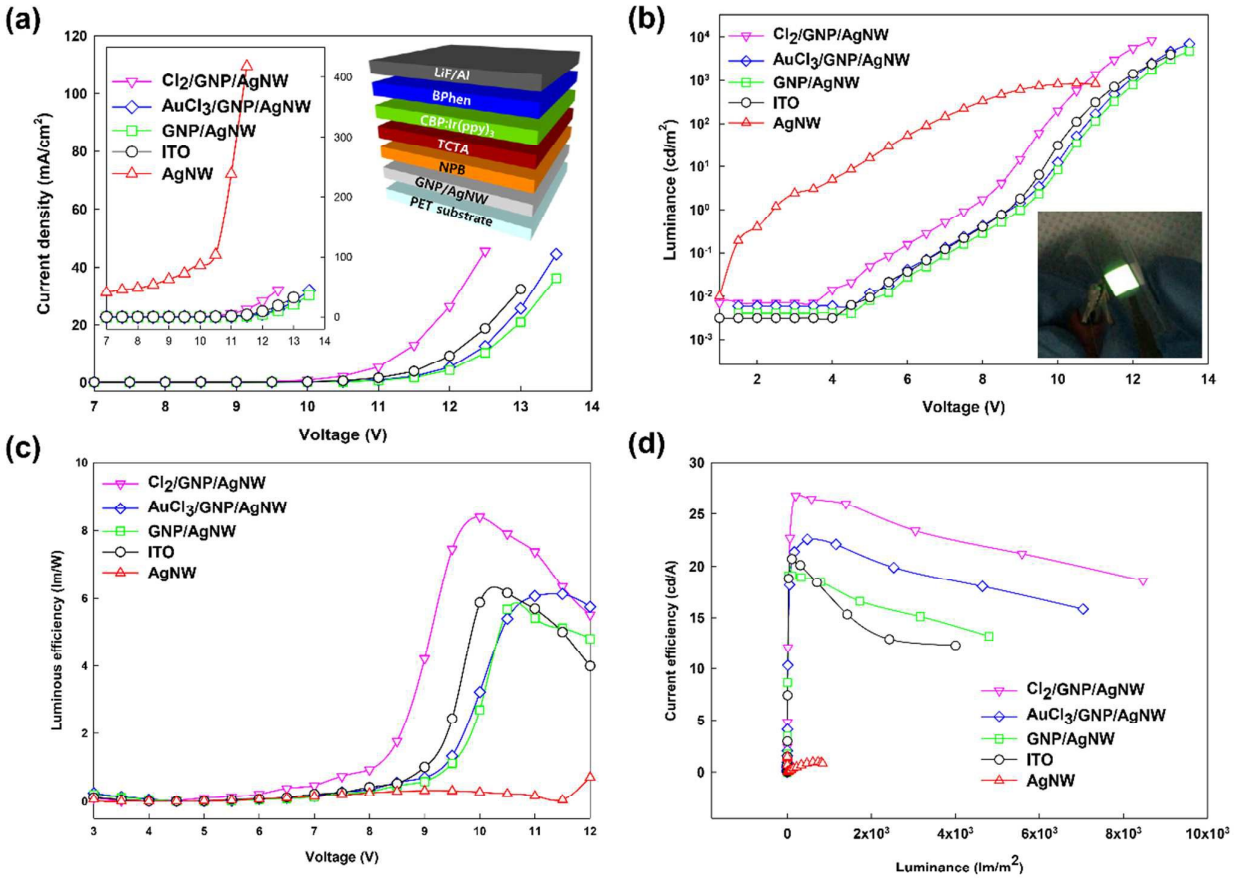

Fig. 8 Device structure and performance of OLED devices with the anodes made of doped-GNP/AgNW, undoped-GNP/AgNW, ITO, and AgNW. a) current densities, b) luminance, c) luminous efficiencies, and d) current efficiencies of OLED devices. The right-insets of a) and b) show the schematic drawing and optical image of light emission from a flexible OLED, respectively.

hybrid electrodes exhibited turn-on voltages from the highest to the lowest in the order of undoped, $AuCl_3$-doped, and Cl_2-doped. Moreover, the turn-on voltage of the OLED device with the Cl_2 plasma-doped GNP/AgNW electrode on PET was lower than that of the OLED device with the ITO on PET electrode. The left-hand inset of Fig. 8a shows the current density as a function of the voltage, including that for an OLED device fabricated with the embedded AgNW electrode. Due to the non-uniform coverage of the AgNW on the PET substrate, a high electric field was concentrated on the local area covered with AgNWs and, therefore, a high leakage current was observed at low voltages even though the OLED device appears to turn on at a low voltage.

Fig. 8b, c, and d show the luminance, luminous efficiencies (LEs) and current efficiencies (CEs), respectively, of the fabricated OLED devices. The right-hand inset of Fig. 8b shows the light-emission performance of a flexible OLED device fabricated with a Cl_2-doped GNP/AgNW electrode on PET under bending to a radius of around 5 mm. At any given voltage, the trends in the luminance and LEs of the fabricated OLED devices were similar to those of the current densities shown in Fig. 8a. That is, the best performances were observed for a device fabricated with a Cl_2-doped hybrid GNP/AgNW electrode. The Cl_2-doped GNP/AgNW electrode exhibits maximum LE values of 8.39 $lm \cdot W^{-1}$, representing 47.7 % of the improvement relative to an OLED device fabricated with the ITO on PET electrode (LE = 6.16 $lm \cdot W^{-1}$). In the case of the undoped GNP/AgNW electrode, the maximum LE value was 5.68 $lm \cdot W^{-1}$, while the corresponding value for $AuCl_3$ doping was 6.13 $lm \cdot W^{-1}$. In the case of the OLED device fabricated with the AgNW electrode embedded in PET, although the luminance at a given voltage was high due to the local area emission resulting from the non-uniform coverage of the AgNW on the OLED surface, the current and luminous efficiencies were extremely low.

Fig. 8d shows the current efficiencies as a function of the luminance. For any given luminance, due to the increase in the work functions of the anodes, the current efficiencies were increased in the order of embedded AgNW, ITO, undoped GNP/AgNW, $AuCl_3$-doped GNP/AgNW, and Cl_2-doped GNP/AgNW. Therefore, the OLED device fabricated with the Cl_2-doped GNP/AgNW electrode exhibited the best characteristics.

Conclusions

View Article Online
DOI: 10.1039/C7NR08078F

We developed a method of fabricating flexible transparent conductive electrodes (TCEs) composed of embedded GNP/AgNW, for application to flexible OLED devices, with excellent physical and electrical properties. Although AgNWs have been widely investigated for use in flexible TCEs and have been found to exhibit excellent conductivity and transmittance, their practical application as the anodes of flexible OLEDs has been limited by their low work function, the nonconductive areas among the NWs, and their high surface roughness. As a result of hybridization with GNP and embedding in a flexible substrate, these limitations of AgNWs, as well as those of CVD graphene, were overcome in the present study. The embedded hybrid GNP/AgNW electrode was found to exhibit an excellent optical transmittance of 87.6 % for a sheet resistance of 12 Ω/sq, an excellent RMS surface roughness of 0.64 nm, and excellent R_{P-V} of 8.47 nm. In addition, the hybrid flexible electrode showed an extremely small resistance increase of ≤ 0.5 % under static bending to a radius of 5 mm and small resistance increase of < 4 % under cyclic bending over 100,000 bending cycles. For comparison, the brittleness of an ITO on PET electrode with a sheet resistance of 12 Ω/sq and an optical transmittance of 86.5 % caused a significant increase in the resistance under both static and cyclic bending, that is, > 29.8 % for static bending to a radius of 5 mm and > 2800 % for 100,000 bending cycles. Furthermore, by hybridizing GNP with AgNW, the stretchability of a GNP/AgNW electrode was greatly enhanced, relative to an AgNW electrode. Compared to an OLED fabricated with an embedded hybrid undoped GNP/AgNW electrode, that with an ITO on PET electrode exhibited similar electrical properties while that with an embedded AgNW electrode was significantly less efficient. The doping of the hybrid electrode with $AuCl_3$ and Cl_2 plasma enhanced the work function of the GNP from 4.52 eV (undoped) to 4.75 and 5.26 eV, respectively, resulting in improvements in the LE of the OLED device of as much as 36.2 %. In addition to the remarkable properties of the proposed hybrid GNP/AgNW transparent flexible electrode, the ease of its production makes it a promising candidate for application not only to OLEDs, but also to various other flexible optoelectronic devices such as organic photovoltaics and photodetectors.

Conflicts of interest

There are no conflicts to declare

Acknowledgements

This study was supported by the Nano Material Technology Development Program through the National Research Foundation of Korea (NRF), funded by the Ministry of Education, Science and Technology (2016M3A7B4910429). It was also supported by the Ministry of Trade, Industry and Energy (MOTIE) (10048504) and the Korea Semiconductor Research Consortium (KSRC) support program for the development of future semiconductor devices.

Notes and references

1 K. S. Novoselov, A. K. Geim, S. V. Morozov, D. Jiang, Y. Zhang, S. V. Dubonos, I. V. Grigorieva and A. A. Firsov, *Science*, 2004, **306**, 666-669.
2 A. K. Geim and K. S. Novoselov, *Nat. Mater.*, 2007, **6**, 183-191.
3 A. A. Balandin, S. Ghosh, W. Bao, I. Calizo, D. Teweldebrhan, F. Miao and C. N. Lau, *Nano Lett.*, 2008, **8**, 902-907.
4 C. Lee, X. Wei, J. W. Kysar and J. Hone, *Science*, 2008, **321**, 385-388.
5 M. D. Stoller, S. Park, Y. Zhu, J. An and R. S. Ruoff, *Nano Lett.*, 2008, **8**, 3498-3502.
6 X. Li, Y. Zhu, W. Cai, M. Borysiak, B. Han, D. Chen, R. D. Piner, L. Colombo and R. S. Ruoff, *Nano Lett.*, 2009, **9**, 4359-4363.
7 S. Bae, H. Kim, Y. Lee, X. Xu, J.-S. Park, Y. Zheng, J. Balakrishnan, T. Lei, H. R. Kim and Y. I. Song, *Nat Nanotechnol.*, 2010, **5**, 574-578.
8 L. Gomez De Arco, Y. Zhang, C. W. Schlenker, K. Ryu, M. E. Thompson and C. Zhou, *ACS nano*, 2010, **4**, 2865-2873.
9 G. Jo, M. Choe, C.-Y. Cho, J. H. Kim, W. Park, S. Lee, W.-K. Hong, T.-W. Kim, S.-J. Park and B. H. Hong, *Nanotechnology*, 2010, **21**, 175201.
10 S. P. Pang, Y. Hernandez, X. L. Feng and K. Mullen, *Adv. Mater.*, 2011, **23**, 2779-2795.
11 T.-H. Han, Y. Lee, M.-R. Choi, S.-H. Woo, S.-H. Bae, B. H. Hong, J.-H. Ahn and T.-W. Lee, *Nat. Photonics*, 2012, **6**, 105-110.
12 A. Reina, X. Jia, J. Ho, D. Nezich, H. Son, V. Bulovic, M. S. Dresselhaus and J. Kong, *Nano Lett.*, 2008, **9**, 30-35.
13 J. W. Suk, A. Kitt, C. W. Magnuson, Y. Hao, S. Ahmed, J. An, A. K. Swan, B. B. Goldberg and R. S. Ruoff, *ACS nano*, 2011, **5**, 6916-6924.
14 Y. Wang, Y. Zheng, X. Xu, E. Dubuisson, Q. Bao, J. Lu and K. P. Loh, *ACS nano*, 2011, **5**, 9927-9933.
15 J. S. Oh, K. N. Kim and G. Y. Yeom, *J. Nanosci. Nanotechno.*, 2014, **14**, 1120-1133.
16 I. N. Kholmanov, C. W. Magnuson, A. E. Aliev, H. Li, B. Zhang, J. W. Suk, L. L. Zhang, E. Peng, S. H. Mousavi, A. B. Khanikaev, R. Piner, G. Shvets and R. S. Ruoff, *Nano Lett.*, 2012, **12**, 5679-5683.
17 S. Yao and Y. Zhu, *Adv. Mater.*, 2015, **27**, 1480-1511.
18 M. S. Lee, K. Lee, S. Y. Kim, H. Lee, J. Park, K. H. Choi, H. K. Kim, D. G. Kim, D. Y. Lee, S. Nam and J. U. Park, *Nano Lett.*, 2013, **13**, 2814-2821.
19 S. Stankovich, D. A. Dikin, R. D. Piner, K. A. Kohlhaas, A. Kleinhammes, Y. Jia, Y. Wu, S. T. Nguyen and R. S. Ruoff, *Carbon*, 2007, **45**, 1558-1565.
20 H. A. Becerril, J. Mao, Z. Liu, R. M. Stoltenberg, Z. Bao and Y. Chen, *ACS nano*, 2008, **2**, 463-470.
21 D. R. Dreyer, S. Park, C. W. Bielawski and R. S. Ruoff, *Chem. Soc. Rev.*, 2010, **39**, 228-240.
22 D. C. Marcano, D. V. Kosynkin, J. M. Berlin, A. Sinitskii, Z. Sun, A. Slesarev, L. B. Alemany, W. Lu and J. M. Tour, *ACS nano*, 2010, **4**, 4806-4814.
23 M. Agostini, L. G. Rizzi, G. Cesareo, V. Russo and J. Hassoun, *Adv. Mater. Interfaces*, 2015, **2**.
24 R. Zacharia, H. Ulbricht and T. Hertel, *Phys. Rev. B*, 2004, **69**, 155406.
25 D. Konios, M. M. Stylianakis, E. Stratakis and E. Kymakis, *J. Colloid Interface Sci.*, 2014, **430**, 108-112.
26 M. Ayan-Varela, J. Paredes, S. Villar-Rodil, R. Rozada, A. Martinez-Alonso and J. Tascón, *Carbon*, 2014, **75**, 390-400.

View Article Online
DOI: 10.1039/C7NR08078F

27 C. Zhao, L. Xing, J. Xiang, L. Cui, J. Jiao, H. Sai, Z. Li and F. Li, *Particuology*, 2014, **17**, 66-73.
28 S. Borini, R. White, D. Wei, M. Astley, S. Haque, E. Spigone, N. Harris, J. Kivioja and T. Ryhanen, *ACS nano*, 2013, **7**, 11166-11173.
29 D. Parviz, S. D. Metzler, S. Das, F. Irin and M. J. Green, *Small*, 2015, **11**, 2661-2668.
30 I. K. Moon, J. I. Kim, H. Lee, K. Hur, W. C. Kim and H. Lee, *Sci. Rep.*, 2013, **3**, 1038-1045.
31 E. Kymakis, K. Savva, M. M. Stylianakis, C. Fotakis and E. Stratakis, *Adv. Funct. Mater.*, 2013, **23**, 2742-2749.
32 X. Liu, H. Kim and L. J. Guo, *Org. Electron.*, 2013, **14**, 591-598.
33 G. Eda, G. Fanchini and M. Chhowalla, *Nat. Nanotechnol.*, 2008, **3**, 270-274.
34 S. Pei and H.-M. Cheng, *Carbon*, 2012, **50**, 3210-3228.
35 S. Park, J. An, J. R. Potts, A. Velamakanni, S. Murali and R. S. Ruoff, *Carbon*, 2011, **49**, 3019-3023.
36 C.-Y. Su, Y. Xu, W. Zhang, J. Zhao, A. Liu, X. Tang, C.-H. Tsai, Y. Huang and L.-J. Li, *Acs Nano*, 2010, **4**, 5285-5292.
37 X. Wang, L. Zhi and K. Müllen, *Nano Lett.*, 2008, **8**, 323-327.
38 J. A. King, D. R. Klimek, I. Miskioglu and G. M. Odegard, *J. Appl. Polym. Sci.*, 2013, **128**, 4217-4223.
39 S. Y. Kim, Y. J. Noh and J. Yu, *Composites Part A*, 2015, **69**, 219-225.
40 H. Wu, B. Rook and L. T. Drzal, *Polym. Compos.*, 2013, **34**, 426-432.
41 A. M. Dimiev, G. Ceriotti, A. Metzger, N. D. Kim and J. M. Tour, *ACS nano*, 2015, **10**, 274-279.
42 D. Cai and M. Song, *J. Mater. Chem.*, 2007, **17**, 3678-3680.
43 L. M. Viculis, J. J. Mack, O. M. Mayer, H. T. Hahn and R. B. Kaner, *J. Mater. Chem.*, 2005, **15**, 974-978.
44 J. Li, L. Vaisman, G. Marom and J.-K. Kim, *Carbon*, 2007, **45**, 744-750.
45 J. Li, M. L. Sham, J.-K. Kim and G. Marom, *Compos. Sci. Technol.*, 2007, **67**, 296-305.
46 X. Li, G. Zhang, X. Bai, X. Sun, X. Wang, E. Wang and H. Dai, *Nat. Nanotechnol.*, 2008, **3**, 538-542.
47 J. Xu, I. Y. Jeon, J. M. Seo, S. Dou, L. Dai and J. B. Baek, *Adv. Mater.*, 2014, **26**, 7317-7323.
48 M. Kim, D. Y. Kim, Y. Kang and O. O. Park, *RSC Adv.*, 2015, **5**, 3299-3305.
49 W. F. Chen, J. M. Schneider, K. Sasaki, C. H. Wang, J. Schneider, S. Iyer, S. Iyer, Y. Zhu, J. T. Muckerman and E. Fujita, *ChemSusChem*, 2014, **7**, 2414-2418.
50 B. Li and W.-H. Zhong, *J. Mater. Sci.*, 2011, **46**, 5595-5614.
51 R. Sengupta, M. Bhattacharya, S. Bandyopadhyay and A. K. Bhowmick, *Prog. Polym. Sci.*, 2011, **36**, 638-670.
52 L.-Y. Chen, H. Konishi, A. Fehrenbacher, C. Ma, J.-Q. Xu, H. Choi, H.-F. Xu, F. E. Pfefferkorn and X.-C. Li, *Scripta Mater.*, 2012, **67**, 29-32.
53 A. Yu, P. Ramesh, X. Sun, E. Bekyarova, M. E. Itkis and R. C. Haddon, *Adv. Mater.*, 2008, **20**, 4740-4744.
54 J. Li, J.-K. Kim and M. L. Sham, *Scripta Mater.*, 2005, **53**, 235-240.
55 S. Araby, L. Zhang, H.-C. Kuan, J.-B. Dai, P. Majewski and J. Ma, *Polymer*, 2013, **54**, 3663-3670.
56 J. S. Park, S. M. Cho, W. J. Kim, J. Park and P. J. Yoo, *ACS Appl. Mater. Interfaces*, 2011, **3**, 360-368.
57 Q. Zheng, W. H. Ip, X. Lin, N. Yousefi, K. K. Yeung, Z. Li and J.-K. Kim, *ACS Nano*, 2011, **5**, 6039-6051.
58 V. H. Pham, T. V. Cuong, S. H. Hur, E. W. Shin, J. S. Kim, J. S. Chung and E. J. Kim, *Carbon*, 2010, **48**, 1945-1951.
59 S. J. Wang, Y. Geng, Q. Zheng and J.-K. Kim, *Carbon*, 2010, **48**, 1815-1823.
60 D. W. Lee, T.-K. Hong, D. Kang, J. Lee, M. Heo, J. Y. Kim, B.-S. Kim and H. S. Shin, *J. Mater. Chem.*, 2011, **21**, 3438-3442.
61 Q. B. Zheng, M. M. Gudarzi, S. J. Wang, Y. Geng, Z. Li and J.-K. Kim, *Carbon*, 2011, **49**, 2905-2916.
62 J. Wang, M. Liang, Y. Fang, T. Qiu, J. Zhang and L. Zhi, *Adv. Mater.*, 2012, **24**, 2874-2878.